Draft version October 7, 2024
Typeset using LaTeX twocolumn style in AASTeX631

Chemically Self-Consistent Modeling of the Globular Cluster NGC 2808 and its Effects on the Inferred Helium Abundance of Multiple Stellar Populations

Emily M. Boudreaux,[1] Brian C. Chaboyer,[1] Amanda Ash,[2] Renata Edaes Hoh,[1] and Gregory Feiden[2]

[1] Department of Physics and Astronomy, Dartmouth College, Hanover, NH 03755, USA
[2] Department of Physics and Astronomy, University of North Georgia, Dahlonega, GA 30533, USA

ABSTRACT

The helium abundances in the multiple populations that are now known to comprise all closely studied Milky Way globular clusters are often inferred by fitting isochohrones generated from stellar evolutionary models to globular cluster photometry. It is therefore important to build stellar models that are chemically self-consistent in terms of their structure, atmosphere, and opacity. In this work we present the first chemically self-consistent stellar models of the Milky Way globular cluster NGC 2808 using MARCS model atmospheres, OPLIB high-temperature radiative opacities, and AESOPUS low-temperature radiative opacities. These stellar models were fit to the NGC 2808 photometry using `Fidanka` , a new software tool that was developed to optimally fit cluster photometry to isochrones and for population synthesis. `Fidanka` can determine, in a relatively unbiased way, the ideal number of distinct populations that exist within a dataset and then fit isochrones to each population. We achieve this outcome through a combination of Bayesian Gaussian Mixture Modeling and a novel number density estimation algorithm. Using `Fidanka` and F275W-F814W photometry from the Hubble UV Globular Cluster Survey we find that the helium abundance of the second generation of stars in NGC 2808 is higher than the first generation by $15 \pm 3\%$. This is in agreement with previous studies of NGC 2808. **This work, along with previous work by Dotter et al. (2015) focused on NGC 6752, demonstrates that chemically self-consistent models of globular clusters do not significantly alter inferred helium abundances, and are therefore unlikely to be worth the significant additional time investment.**

Keywords: Globular Clusters (656), Stellar evolutionary models (2046)

1. INTRODUCTION

Globular clusters (GCs) are among the oldest observable objects in the universe (Peng et al. 2011). They are characterized by high densities with typical half-light radii of ≤10 pc (van den Bergh 2010), and typical masses ranging from 10^4–10^5 $M_\odot$ (Brodie & Strader 2006) — though some GCs are significantly larger than these typical values (e.g. ω Cen, Richer et al. 1991). GCs provide a unique way to probe stellar evolution **(Kalirai & Richer 2010)**, galaxy formation models (Boylan-Kolchin 2018; Kravtsov & Gnedin 2005), and dark matter halo structure (Hudson & Robison 2018).

Corresponding author: Emily M. Boudreaux
emily.m.boudreaux.gr@dartmouth.edu,
emily@boudreauxmail.com

The traditional view of globular clusters is that they consist of a single stellar population (SSP, in some publications this is referred to as a Simple Stellar Population). This view was supported by spectroscopically uniform heavy element abundances (Carretta et al. 2010; Bastian & Lardo 2018) across most clusters (M54 and ωCen are notable exceptions, see Marino et al. (2015) for further details), and the lack of evidence for multiple stellar populations (MPs) in past color-magnitude diagrams of GCs (i.e. Sandage 1953; Alcaino 1975). However, over the last 40 years non-trivial star-to-star light-element abundance variations have been observed (i.e. Smith 1987) and, in the last two decades, it has been definitively shown that most, if not all, Milky Way GCs have MPs (Gratton et al. 2004, 2012; Piotto et al. 2015). The lack of photometric evidence for MPs prior to the 2000, can be attributed to the more narrow color bands available, until very recently, to ground-based photometric surveys (Milone et al. 2017).

The prevalence of multiple populations in GCs is so distinct that the proposed definitions for what constitutes a globular cluster now often center on the existence of MPs (e.g. Carretta et al. 2010). Whereas people have have often tried to categorize objects as GCs through relations between half-light radius, density, and surface brightness profile, in fact many objects which are generally thought of as GCs don't cleanly fit into these cuts (Peebles & Dicke 1968; Brown et al. 1991, 1995; Bekki & Chiba 2002). Consequently, Carretta et al. (2010) proposed a definition of GCs based on observed chemical inhomogeneities in their stellar populations. The modern understanding of GCs then is not simply that of a dense cluster of stars that may have chemical inhomogeneities and multiple populations; rather, it is one where those chemical inhomogeneities and multiple populations themselves are the defining elements of a GC.

All Milky Way globular clusters studied in detail show populations enriched in He, N, and Na while also being depleted in O and C (Piotto et al. 2015; Bastian & Lardo 2018). **Further, studies of Magellenic Cloud massive clusters have shown that these light element abundance variations exist in clusters as young as ~ 2 Gyr but not in younger clusters (Martocchia et al. 2019) while there is also evidence of nitrogen variability in the ~ 1.5 Gyr old cluster NGC 1783 (Cadelano et al. 2022)**. These light element abundance patterns also are not strongly correlated with variations in heavy element abundance, resulting in spectroscopically uniform Fe abundances between populations (**though recent work indicates that there may be [Fe/H] variations within the first population, e.g. Legnardi et al. 2022; Lardo et al. 2022)** . Further, high-resolution spectral studies reveal anti-correlations between N-C abundances, Na-O abundances, and potentially Al-Mg (Sneden et al. 1992; Gratton et al. 2012). Typical stellar fusion reactions can deplete core oxygen; however, the observed abundances of Na, Al, and Mg cannot be explained by the CNO cycle (Prantzos et al. 2007). Consequently, globular cluster populations must be formed by some novel means.

Formation channels for these multiple populations remain a point of debate among astronomers. Most proposed formation channels consist of some older, more massive population of stars polluting the pristine cluster media before a second population forms, now enriched in heavier elements which they themselves could not have generated (for a detailed review see Gratton et al. 2012). The four primary candidates for these polluters are asymptotic giant branch stars (AGBs, Ventura et al. 2001; D'Ercole et al. 2010), fast rotating massive stars (FRMSs, Decressin et al. 2007), super massive stars (SMSs, Denissenkov & Hartwick 2014), and massive interacting binaries (MIBs, de Mink et al. 2009; Bastian & Lardo 2018).

Hot hydrogen burning (i.e. proton capture), material transport to the surface, and material ejection into the intra-cluster media are features of each of these models and consequently they can all be made to *qualitatively* agree with the observed elemental abundances. However, none of the standard models can currently account for all specific abundances (Gratton et al. 2012). AGB and FRMS models are the most promising; however, both models have difficulty reproducing severe O depletion (Ventura & D'Antona 2009; Decressin et al. 2007). Moreover, AGB and FRMS models require significant mass loss ($\sim 90\%$) between cluster formation and the current epoch — implying that a significant fraction of halo stars formed in GCs (Renzini 2008; D'Ercole et al. 2008; Bastian & Lardo 2015).

In addition to the light-element anti-correlations observed, it is also known that second populations are significantly enhanced in helium (Piotto et al. 2007, 2015; Latour et al. 2019). Depending on the cluster, helium mass fractions as high as $Y = 0.4$ have been inferred (e.g Milone et al. 2015a). However, due to both the relatively high and tight temperature range of partial ionization for He and the efficiency of gravitational settling in core helium burning stars, the initial He abundance of globular cluster stars cannot be observed; consequently, the evidence for enhanced He in GCs originates from comparison of theoretical stellar isochrones to the observed color-magnitude-diagrams of globular clusters. Therefore, a careful handling of chemistry is essential when modeling with the aim of discriminating between MPs; yet only a very limited number of GCs have been studied with chemically self-consistent (structure and atmosphere) isochrones (e.g. Dotter et al. 2015, NGC 6752).

NGC 2808 is the prototype globular cluster to host multiple populations. Various studies since 2007 have identified that it may host anywhere from two to five stellar populations. These populations have been identified both spectroscopically (i.e. Carretta et al. 2004; Carretta 2006; Carretta et al. 2010; Gratton et al. 2011; Carretta 2015; Hong et al. 2021) and photometrically (i.e. Piotto et al. 2007, 2015; Milone et al. 2015a, 2017; Pasquato & Milone 2019). Note that recent work (Valle et al. 2022) calls into question the statistical significance of the detections of more than two populations in the spectroscopic data. Here we present **the first stel-**

lar structure and evolutionary models built in a chemically self-consistent manner of NGC 2808.

We model the photometry of the **primordial population (hereafter P1) and the helium enriched population (hereafter P2). Milone et al. (2015a) identifies five populations within NGC 2808, given that the aim of this work is not to identify sub-populations; rather, to measure the effect that chemical self consistant stellar structure and evolutionary have on the inferred helium abundance for the two most extreme cases, we do not consider more than those two populations.** We use archival photometry from the Hubble UV Globular Cluster Survey (HUGS) (Piotto et al. 2015; Milone et al. 2017) in the F275W and F814W passbands to characterize multiple populations in NGC 2808 (Milone et al. 2015a,b) (This data is available on MAST, Piotto 2018). Additionally, we present a likelihood analysis of the photometric data of NGC 2808 to determine the number of populations present in the cluster.

2. CHEMICAL CONSISTENCY

There are three primary areas in which the stellar models must be made chemically consistent: the atmospheric boundary conditions, the opacities, and interior abundances. The interior abundances are relatively easily handled by adjusting parameters within our stellar evolutionary code. However, the other two areas are more difficult to make consistent. Atmospheric boundary conditions and opacities must both be calculated with a consistent set of chemical abundances outside of the stellar evolution code. **Nearly all prior efforts at modeling multiple stellar populations in globular clusters have adjusted the abundances used in the atmospheric interior models, and in the high temperature opacities, but have not self-consistently modified the corresponding low-temperature opacities and surface boundary conditions, as these are found from stellar atmosphere codes, and not the stellar interior codes which are used to create stellar models and isochrones. In this work, as in Dotter (2016), the stellar interior models are chemically self-consistent with the stellar atmosphere models.** For evolution, we use the Dartmouth Stellar Evolution Program (DSEP) (Dotter et al. 2008), a well-tested 1D stellar evolution code which has a particular focus on modeling low mass stars (≤ 2 M$_{\odot}$)

2.1. *Atmospheric Boundary Conditions*

Certain assumptions, primarily that the radiation field is at equilibrium and radiative transport is diffusive (Salaris & Cassisi 2005), made in stellar structure codes, such as DSEP, are valid when the optical depth of a star is large. However, in the atmospheres of stars, the number density of particles drops low enough and the optical depth consequently becomes small enough that these assumptions break down, and separate, more physically motivated, plasma- modeling code is required. Generally, structure code will use tabulated atmospheric boundary conditions generated by these specialized codes, such as ATLAS9 (Kurucz 1993), PHOENIX (Husser et al. 2013), MARCS (Gustafsson et al. 2008), and MPS-ATLAS (Kostogryz et al. 2023). Often, because the boundary conditions are expensive to compute, they are not updated as interior abundances vary.

One key element when building chemically self-consistent models of NGC 2808 is the incorporation of new atmospheric boundary conditions with the same elemental abundances as the structure code. We use atmospheres generated from the `MARCS` grid of model atmospheres (Plez 2008). `MARCS` provides one-dimensional, hydrostatic, plane-parallel and spherical LTE atmospheric models (Gustafsson et al. 2008). Model atmospheres are made to match the spectroscopically measured elemental abundances of Milone et al. (2015a) populations A&E. Moreover, for each population, atmospheres with various helium mass fractions are generated. These range from Y=0.24 to Y=0.36 in steps of 0.03. All atmospheric models are computed to an optical depth of $\tau = 100$ where their temperature and pressure serve as boundary conditions for the structure code. In general, enhancing helium in the atmosphere has only a small impact on the atmospheric temperature profile, while leading to a drop in the pressure by $\sim 10 - 20\%$.

2.2. *Opacities*

In addition to the atmospheric boundary conditions, both the high and low temperature opacities used by DSEP must be made chemically consistent. Here we use OPLIB high temperature opacity tables (Colgan et al. 2016) retrieved using the TOPS web-interface. Retrival of high termperature opacities is done using `pyTOPSScrape`, first introduced in Boudreaux & Chaboyer (2023). Low temperature opacity tables are retrieved from the Aesopus 2.0 web-interface (Marigo & Aringer 2009; Marigo et al. 2022). Ideally, these opacities would be the same used in the atmospheric models. However, the opacities used in the MARCS models are not publicly available. As such, we use the opacities provided by the TOPS and Aesopus 2.0 web-interfaces.

3. STELLAR MODELS

We use the Dartmouth Stellar Evolution Program (DSEP, Dotter et al. 2008) to generate stellar models. DSEP is a one-dimensional stellar evolution code that includes a mixing length model of convection, gravitational settling, and diffusion. Using the solar composition presented in (Grevesse et al. 2007) (GAS07), MARCS model atmosphers, OPLIB high temperature opacities, and AESOPUS 2.0 low temperautre opacities we find a solar calibrated mixing length parameter, α_{MLT}, of $\alpha_{MLT} = 1.901$. **Abundance measurments are derived from populations A&E in Milone et al. (2015a) (for P1 and P2 respectivley).**

We use DSEP to evolve stellar models ranging in mass from 0.3 to 2.0 solar masses from the fully convective pre-main sequence to the tip of the red giant branch. Below 0.7 $M_{\odot}$ we evolve a model every 0.03 $M_{\odot}$ and above 0.7 $M_{\odot}$ we evolve a model every 0.05 $M_{\odot}$. We evolve models over a grid of mixing length parameters from $\alpha_{MLT} = 1.0$ to $\alpha_{MLT} = 2.0$ in steps of 0.1. For each mixing length, a grid of models and isochrones were calculated, with chemical compositions consistent with Milone et al. (2015a) populations A and E (see Tables 1 and 1) and a range of helium abundances (Y=0.24, 0.27, 0.30, 0.33, 0.36, and 0.39). In total, 144 sets of isochrones, each with a unique composition and mixing length were calculated. Each model is evolved in DSEP with typical numeric tolerences of one part in 10^7. Each model is allowed a maximum time step of 50 Myr.

For each combination of populations, Y, and α_{MLT} we use the isochrone generation code first presented in Dotter (2016) to generate a grid of isochrones. The isochrone generation code identified equivalent evolutionary points (EEPs) over a series of masses and interpolates between them. The grid of isochrones generated for this work is avalible as a digital supplement to this paper 10.5281/zenodo.10631439. Given the complexity of the parameter space when fitting multiple populations, along with the recent warnings in the literature regarding overfitting datasets (e.g. Valle et al. 2022), we want to develop a more objective way of fitting isochrones to photometry than if we were to mark median ridge line positions by hand.

4. FIDANKA

When fitting isochrones to the clusters with multiple populations we have four main criteria for any method:

- The method must be robust enough to work along the entire main sequence, turn off, and much of the subgiant and red giant branch.

Table 1. Population Composition

Element	P1 (A)	P2 (E)	Element	P1 (A)	P2 (E)
Li	-0.08	—	In	-1.46	—
Be	0.25	—	Sn	-0.22	—
B	1.57	—	Sb	-1.25	—
C	6.87	5.91	Te	-0.08	—
N	6.42	6.69	I	-0.71	—
O	7.87	6.91	Xe	-0.02	—
F	3.43	—	Cs	-1.18	—
Ne	7.12	6.7	Ba	1.05	—
Na	5.11	5.7	La	-0.03	—
Mg	6.86	6.42	Ce	0.45	—
Al	5.21	6.61	Pr	-1.54	—
Si	6.65	6.77	Nd	0.29	—
P	4.28	—	Pm	-99.0	—
S	6.31	5.89	Sm	-1.3	—
Cl	-1.13	4.37	Eu	-0.61	—
Ar	5.59	5.17	Gd	-1.19	—
K	3.9	—	Tb	-1.96	—
Ca	5.21	—	Dy	-1.16	—
Sc	2.02	—	Ho	-1.78	—
Ti	3.82	—	Er	-1.34	—
V	2.8	—	Tm	-2.16	—
Cr	4.51	—	Yb	-1.42	—
Mn	4.3	—	Lu	-2.16	—
Fe	6.37	—	Hf	-1.41	—
Co	3.86	—	Ta	-2.38	—
Ni	5.09	—	W	-1.41	—
Cu	3.06	—	Re	-2.0	—
Zn	2.3	—	Os	-0.86	—
Ga	0.78	—	Ir	-0.88	—
Ge	1.39	—	Pt	-0.64	—
As	0.04	—	Au	-1.34	—
Se	1.08	—	Hg	-1.09	—
Br	0.28	—	Tl	-1.36	—
Kr	0.99	—	Pb	-0.51	—
Rb	0.26	—	Bi	-1.61	—
Sr	0.61	—	Po	-99.0	—
Y	1.08	—	At	-99.0	—
Zr	1.45	—	Rn	-99.0	—
Nb	-0.8	—	Fr	-99.0	—
Mo	-0.38	—	Ra	-99.0	—
Tc	-99.0	—	Ac	-99.0	—
Ru	-0.51	—	Th	-2.2	—
Rh	-1.35	—	Pa	-99.0	—
Pd	-0.69	—	U	-2.8	—

Note—Relative Metal composition used where a(H) = 12. Composition measurments are taken from Milone et al. (2015a) populations A&E (P1 and P2 respectively). Where the relative composition is the the same for both P1 and P2; it is only listed in the P1 column for the sake of visual clarity.

References—Milone et al. (2015a)

Table 2. Population Abundance Ratios

Population	[Fe/H]	[α/Fe]	[C/Fe]	[N/Fe]	[O/Fe]	[r/Fe]	[s/Fe]	C/O	X	Y	Z
A(1)	-1.13	0.32	-0.43	-0.28	0.31	-1.13	-1.13	0.10	0.7285	0.2700	0.00154
E(2)	-1.13	-0.11	-1.39	-0.02	-0.66	-1.13	-1.13	0.10	0.7594	0.240	0.00063

Note—Abundance ratios for populations P1 and P2 in NGC 2808.

References—Milone et al. (2015a)

- Any method should consider photometric uncertainty in the fitting process.
- The method should be model independent, weighting any n number of populations equally.
- The method should be automated and require minimal intervention from the user.

We do not believe that any currently available software is a match for our use case. Therefore, we have developed our own software suite, `Fidanka` . `Fidanka` is a Python package designed to automate much of the process of measuring fiducial lines in CMDs, adhering to the four criteria we lay out above. Primary features of `Fidanka` may be separated into three categories: fiducial line measurement, stellar population synthesis, and isochrone optimization/fitting. Additionally, there are utility functions that are detailed in the `Fidanka` documentation.

4.1. *Fiducial Line Measurement*

`Fidanka` takes a iterative approach to measuring fiducial lines, the first step of which is to make a "guess" as to the fiducial line. This initial guess is calculated by splitting the CMD into magnitude bins, with uniform numbers of stars per bin (so that bins cover a small magnitude range over densely populated regions of the CMD, while covering a much larger magnitude range in sparsely populated regions of the CMD, such as the RGB). A unimodal Gaussian distribution is then fit to the color distribution of each bin, and the resulting mean color is used as the initial fiducial line guess. This rough fiducial line will approximately trace the area of highest density. The initial guess will be used to verticalize the CMD so that further algorithms can work in 1D magnitude bins without worrying about weighting issues caused by varying projections of the evolutionary sequence onto the magnitude axis. Verticalization is performed by taking the difference between the guess fiducial line and the color of each star in the CMD.

If `Fidanka` were to simply apply the same algorithm to the verticalized CMD, then the resulting fiducial line would likely be a re-extraction of the initial fiducial line guess. To avoid this outcome, we take a more robust, number-density based approach that considers the distribution of stars in both color and magnitude space simultaneously. **As an example, in the case of this work,** for each star in the CMD we first use an `introselect` partitioning algorithm to select the 50 nearest stars in F814W vs. F275W-F814W space. **It should be noted that unlike methods using chromosome maps `Fidanka` only considers two filters and therefore might lose access to information better traced by other filters.** To account for the case where the star is at an extreme edge of the CMD, those 50 stars include the star itself (such that we really select 49 stars + 1). We use `qhull`[1] (Barber et al. 1996) to calculate the convex hull of those 50 points. The number density at each star then is defined as $50/A_{hull}$, where A_{hull} is the area of the convex hull. Because we use a fixed number of points per star, and a partitioning algorithm as opposed to a sorting algorithm, this method scales like $\mathcal{O}(n)$, where n is the number of stars in the CMD. This method also intrinsically weights the density of each star equally, as the counting statistics per bin are uniform. We are left with a CMD in which each star has a defined number density (Figure 1).

`Fidanka` can now exploit this density map to fit a better fiducial line to the data, as the density map is far more robust to outliers. There are multiple algorithms that we implement to fit the fiducial line to the color-density profile in each magnitude bin (Figure 2); these are explained in more detail in the `Fidanka` documentation. However, of most relevance here is the Bayesian Gaussian Mixture Modeling (BGMM) method. BGMM is a clustering algorithm that, for some fixed number of n-dimensional Gaussian distributions, K, determines the mean, covariance, and mixing probability (somewhat analogous to amplitude) of each k^{th} distribution, such that the local lower bound of the likelihood of each

[1] https://www.qhull.com

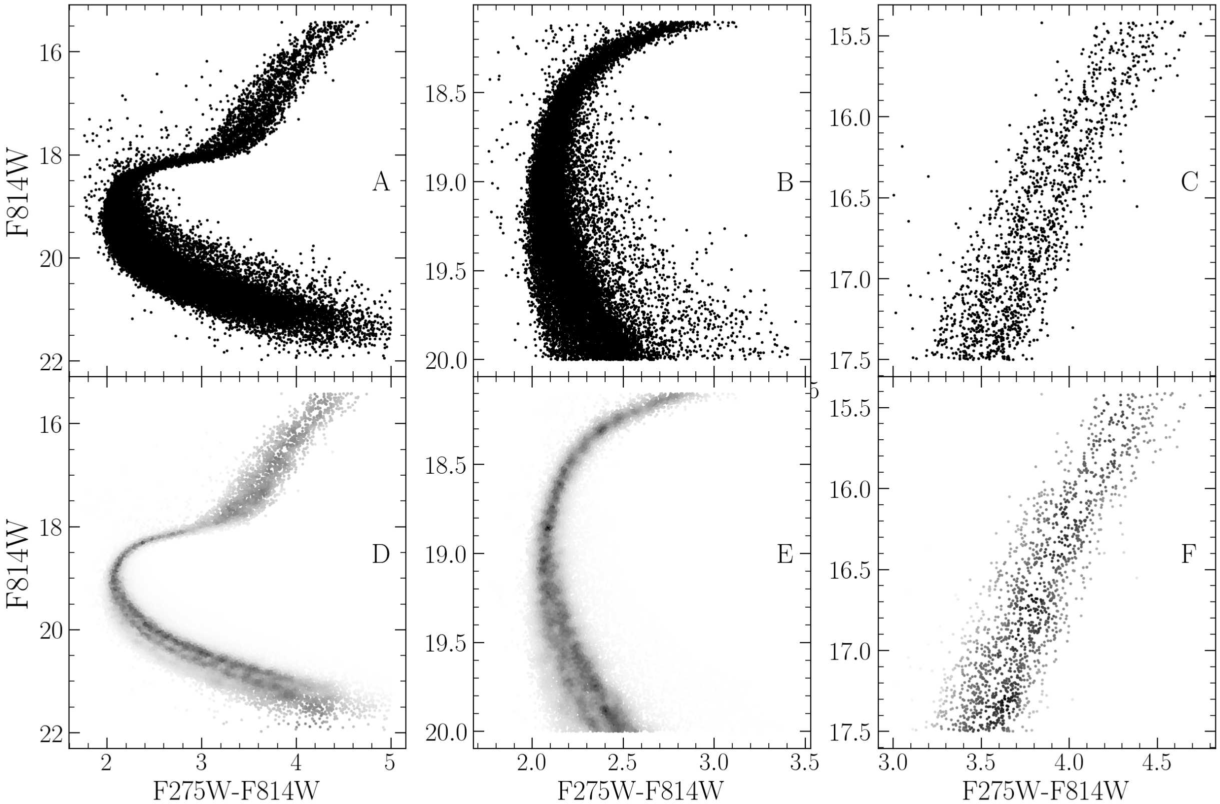

Figure 1. Figures in the top row are the raw CMD, while figures in the bottom row are colored by the density map. Density map demo showing density estimate over different parts of the evolutionary sequence. The left panel shows the density map over the entire evolutionary sequence, while the middle panel shows the density map over the main sequence and the right panel shows the density map over the RGB.

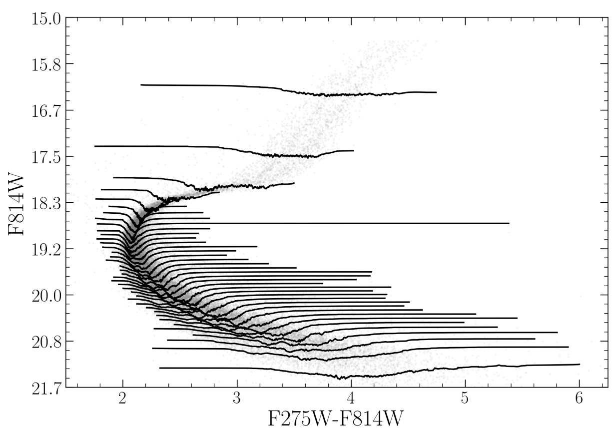

Figure 2. CMD where point brightness is determined by local density. Lines show the density-color profile in each magnitude bin. In this figure adaptive binning targeted 1000 stars per bin

star belonging strongly to a single distribution is maximized.

Maximization is performed using the Dirichlet process, which is a non-parametric Bayesian method of determining the number of Gaussian distributions, K, that best fit the data (Ferguson 1973; Pedregosa et al. 2011). Use of the Dirichlet process allows for dynamic variation in the number of inferred populations from magnitude bin to magnitude bin. Specifically, populations are clearly visually separated from the lower main sequence through the turn off; however, at the turn off and throughout much of the subgiant branch, the two visible populations overlap due to their similar ages (i.e. Jordán et al. 2002). The Dirichlet process allows for the BGMM method to infer a single population in these regions, while inferring two populations in regions where they are clearly separated. More generally, the use of the Dirichlet process removes the need for a prior on the exact number of populations to fit. Rather, the user specifies a upper bound on the number of populations within the cluster. An example bin (F814W = 20.6) is shown in Figure 3.

`Fidanka` 's BGMM method first breaks down the verticalized CMD into magnitude bins with uniform numbers of stars per bin (here we adopt 250). Any stars left over are placed into the final bin. For each bin a BGMM model with a maximum of five populations is fit to the color density profile. The number of popula-

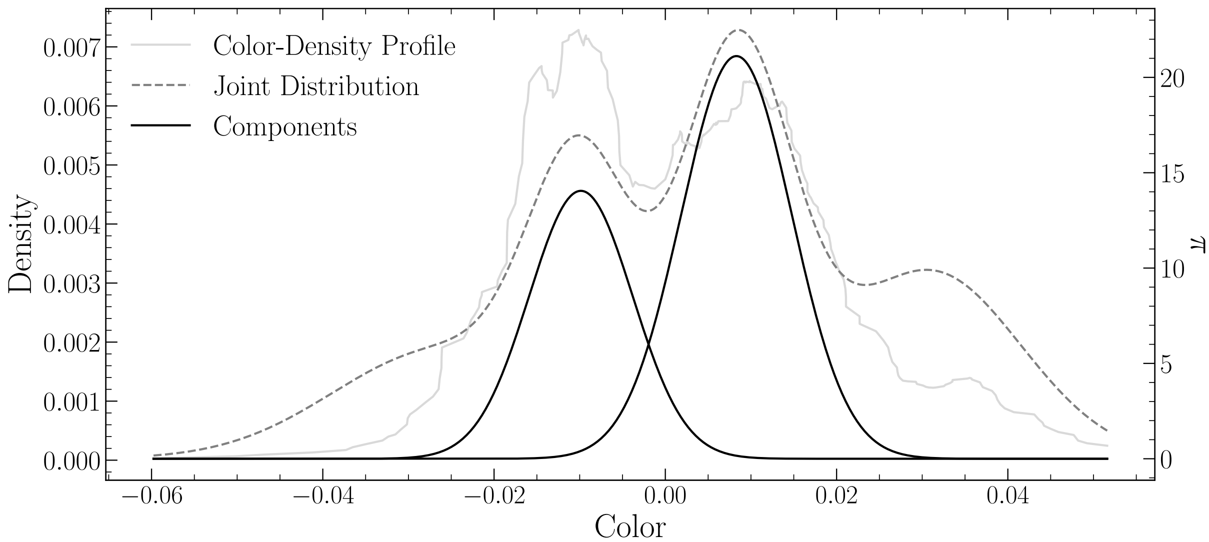

Figure 3. Example of BGMM fit to a magnitude bin. The grey line shows the underlying color-density profile, while the black dashed line shows the joint distribution of each BGMM component. The solid black lines show the two selected components.

tions is then inferred from the weighting parameter (the mixing probability) of each population. If the weighting parameter of any k^{th} components is less than 0.05, then that component is considered to be spurious and removed. Additionally, if the number of populations in the bin above and the bin below are the same, then the number of populations in the current bin is forced to be the same as the number of populations in the bin above. Finally, the initial guess fiducial line is added back to the BGMM inferred line. Figure 4 shows the resulting fiducial line(s) in each magnitude bin for both a verticalized CMD and a non-verticalized CMD. In contrast to other work in the literature where evidence for up to five distinct populations has been found, we only find evidence for two stellar populations.

This method of fiducial line extraction effectively discriminated between multiple populations along the main sequence and RGB of a cluster, while simultaneously allowing for the presence of a single population along the MSTO and subgiant branch.

We can adapt this density map-based BGMM method to consider photometric uncertainties by adopting a simple Monte Carlo approach. Instead of measuring the fiducial line(s) a single time, `Fidanka` can measure the fiducial line(s) many times, resampling the data with replacements each time. For each resampling, `Fidanka` adds a random offset to each filter based on the photometric uncertainties of each star. From these n measurements the mean fiducial line for each sequence can be identified along with upper and lower-bound confidence intervals in each magnitude bin.

4.2. *Stellar Population Synthesis*

While not extensively used in this paper `Fidanka` can, in addition to measuring fiducial lines, perform stellar population synthesis. `Fidanka` 's population synthesis module can generate synthetic stellar populations from a set of MIST-formatted isochrones. This is of primary importance for binary population modeling. The module is also used to generate synthetic CMDs for the purpose of testing the fiducial line extraction algorithms against priors.

`Fidanka` uses MIST-formatted isochrones (Dotter 2016) as input along with distance modulus, B-V color excess, binary mass fraction, and bolometric corrections. An arbitrarily large number of isochrones may be used to define an arbitrary number of populations. Synthetic stars are samples from each isochrone based on a definable probability; For example, it is believed that $\sim 90\%$ of stars in globular clusters are younger population (e.g. Suntzeff & Kraft 1996; Carretta 2013). Based on the metallicity, μ, and E(B-V) of each isochrone, bolometric corrections are taken from bolometric correction tables. Where bolometric correction tables do not include exact metallicities or extinctions a linear interpolation is performed between the two bounding values.

4.3. *Isochrone Optimization*

The optimization routines in `Fidanka` will find the best fit distance modulus, B-V color excess, and binary number fraction for a given set of isochrones. If a single isochrone is provided then the optimization is done by minimizing the χ^2 of the perpendicular distances between an isochrone and a fiducial line. If multiple isochrones are provided then those isochrones are first used to run a stellar population synthesis and gener-

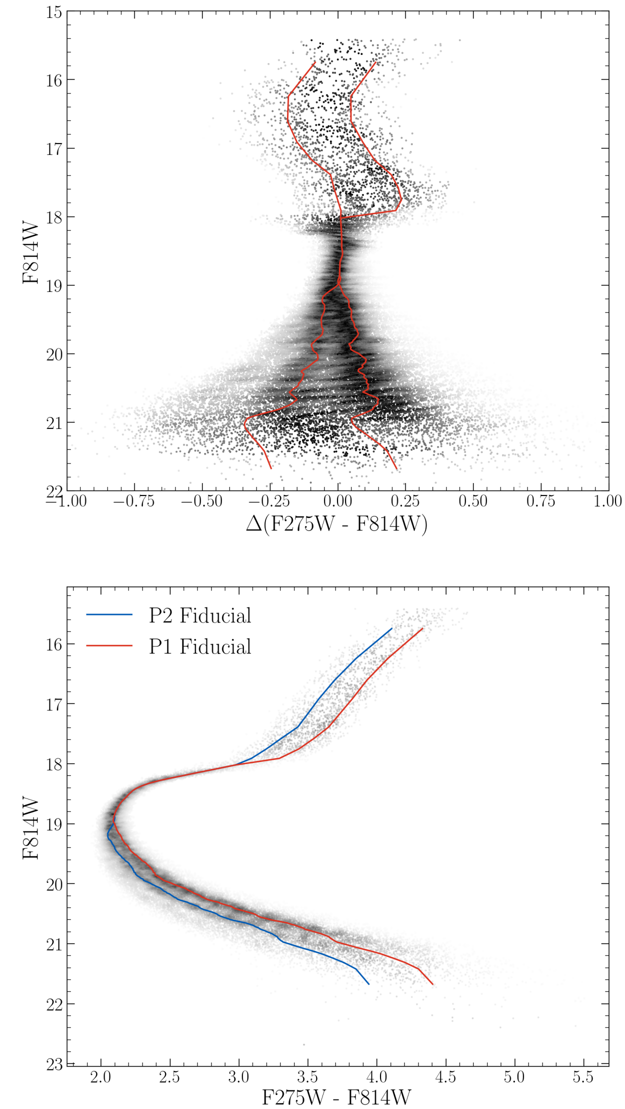

Figure 4. Verticalized CMD (where the color of each data point is subtracted from the color of the fiducial line at that magnitude) where point brightness is determined by density (top). CMD where point brightness is determined by density, calculated fiducial lines are shown (bottom). The data used is from the Hubble Space Telescope UV Legacy Survey of Galactic Globular Clusters.

ate a synthetic CMD. The optimization is then done by minimizing the χ^2 of both the perpendicular distances between and widths of the observed fiducial line and the fiducial line of the synthetic CMD.

4.4. *Fidanka Testing*

In order to validate `Fidanka` we have run a series of injection recovery tests using `Fidanka` 's population synthesis routines to build various synthetic populations and `Fidanka` 's fiducial measurement routines to recover these populations. Each population was generated using the initial mass function given in (Milone et al. 2012) for the redmost population ($\alpha = -1.2$). Further, every population was given a binary population fraction of 10%, distance uniformly sampled between 5000pc and 15000pc, and a B-V color excess uniformly sampled between 0 and 0.1. **`Fidanka` makes use of ACS artificial star tests (Anderson et al. 2008) to model the noise and completness of a synthetic population in passbands covered by those tests. Full details on how `Fidanka` uses artificial star tests may be found on its documentation page**[2] Finally, each synthetic population was generated using a fixed age uniformly sampled between 7 Gyr and 14 Gyr. An example synthetic population, along with its associated best fit isochrone, are shown in Figure 5.

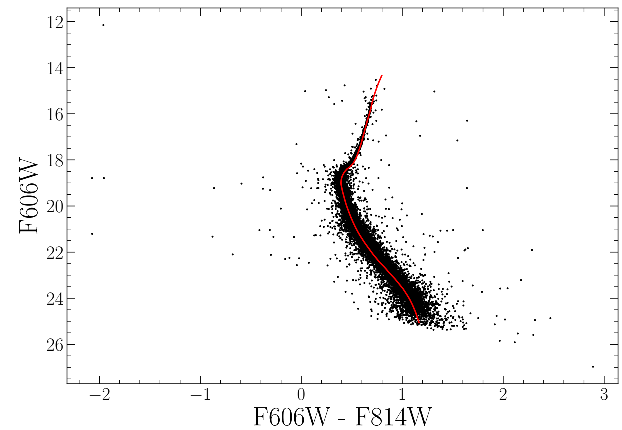

Figure 5. Synthetic population generated by `Fidanka` at 10000pc with E(B-V) = 0, and an age of 12 Gyr along with the best fitting isochrone. The best fit paremeters are derived to be $\mu = 15.13$, E(B-V)=0.001, and an age of 12.33 Gyr.

For each trial we use `Fidanka` to measure the fiducial line and then optimize that fiducial line against the originating isochrone to esimate distance modulus, age, and color B-V excess. Figure 6 is built from 1000 **Monte-Carlo** trials and shows the mean and width of the percent error distributions for μ, A_v, and age. In general `Fidanka` is able to recover distance modulii effectively with age and E(B-V) recovery falling in line with other literature that does not cosider the CMD outside of the main sequence, main sequence turn off, subgiant, and red giant branches. Specifically, it should be noted that `Fidanka` is not set up to model the horizontal branch.

5. ISOCHRONE FITTING

We fit pairs of isochrones to the HUGS data for NGC 2808 using `Fidanka` , as described in §4. **As was men-**

[2] https://tboudreaux.github.io/fidanka/

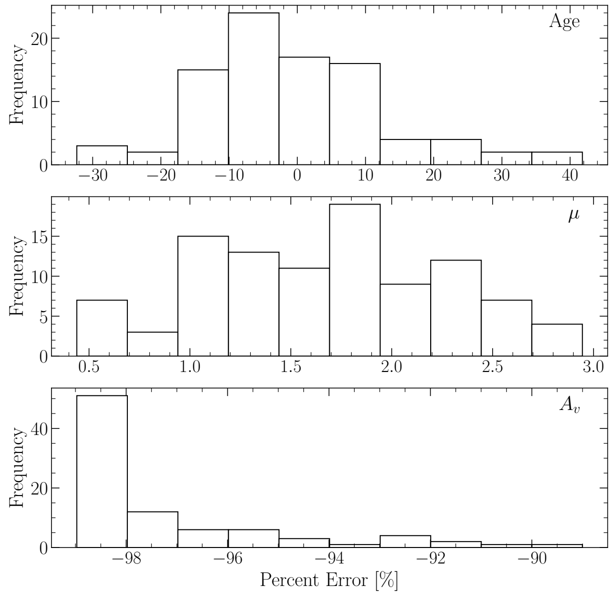

Figure 6. Percent error distribution for each of the three deriver parameters. Note that these values will be sensitive to the magnitude uncertainties of the photometry. Here we made use of the ACS artificial star tests to estimate the uncertanties.

tioned in §4.1, the method used by `Fidanka` only consideres two filters — in the case of this work F275W and F814W — and therefore might be unable to distinguish between populations separated only in the higher-dimensional space of a chromosome map. For further discussion of why we adopt this method, despite it limits, we refer the reader to §5.1. Two isochrones, one for P1 and one for P2 are fit simultaneously. These isochrones are constrained to have distance modulus, μ, and color excess, E(B-V) which agree to within 0.5% and an ages which agree to within 1%. Moreover, we constrain the mixing length, α_{ML}, for any two isochrones in a set to be within 0.5 of one and other. For each isochrone set we optimize μ_{P1}, μ_{P2}, $E(B-V)_{P1}$, $E(B-V)_{P2}$, Age$_{P1}$, and Age_{P2} in order to reduce the χ^2 distance ($\chi^2 = \sum \sqrt{\Delta \mathrm{color}^2 + \Delta \mathrm{mag}^2}$) between the fiducial lines and the isochrones. Because we fit fiducial lines directly, we do not need to consider the binary population fraction, f_{bin}, as a free parameter.

The best fit isochrones are shown in Figure 7 and optimized parameters for these are presented in Table 1. **The initial guess for the age of these populations was locked to 12 Gyr and the initial extinction was locked to 0.5 mag. The initial guess for the distance modulus was determined at run time using a dynamic time warping algorithm to best align the morphologies of the fiducial line with the target isochrone. This algorithm is explained in more detail in the `Fidanka` documentation under the function called `guess_mu`.** We find helium mass fractions that are consistent with those identified in past literature (e.g. Milone et al. 2015a). Note that our helium mass fraction grid has a spacing of 0.03 between grid points and we are therefore unable to resolve between certain proposed helium mass fractions for the younger sequence (for example between 0.37 and 0.39). **We also note that the best fit mixing length parameters which we derive for P1 and P2 do not agree within their uncertainties. This is not surprising, as the much higher mean molecular mass of P2 — when compared to P1, due to population P2's larger helium mass fraction — will result in a steeper adiabatic temperature gradient**.

Past literature (e.g. Milone et al. 2015a, 2018) has found helium mass fraction variation from the redmost to bluemost populations of ~ 0.12. Here we find a helium mass fraction variation of 0.15 that, given the spacing of the helium grid we use *is consistent with these past results.* **The helium mass fractions we derive for P1 and P2 are consistent with those of populations A and E in Milone et al. (2015a); however, populations B+C and D in that study are more prominently separated in the F275W-F814W colorband. The inferred helium mass fractions for P1 and P2 are not consistent with those reported for populations B+C and D.**

5.1. *The Number of Populations in NGC 2808*

In order to estimate the number of populations that ideally fit the NGC 2808 F275W-F814W photometry without overfitting the data we make use of silhouette analysis (Rousseeuw 1987; Shahapure & Nicholas 2020, and in a similar manner to how Valle et al. (2022) perform their analysis of spectroscopic data). We find the average silhouette score for the hypothesizes that there are two, three, four, or five population in each magnitude bin. We preform this analysis over all magnitude using routines built into the standard Python module `sklearn`. Figure 8 (top) shows the silhouette analysis results and that two populations fit the photometry most ideally. This result is in line with what our BGMM model predicts for the majority of the CMD.

While we make use of a purely CMD-based approach in this work, other literature has made use of chromosome maps. These consist of implicitly verticalized pseudo colors. In the chromosome map for NGC 2808 there may be evidence for more than two populations; further, the chromosome maps used include in-

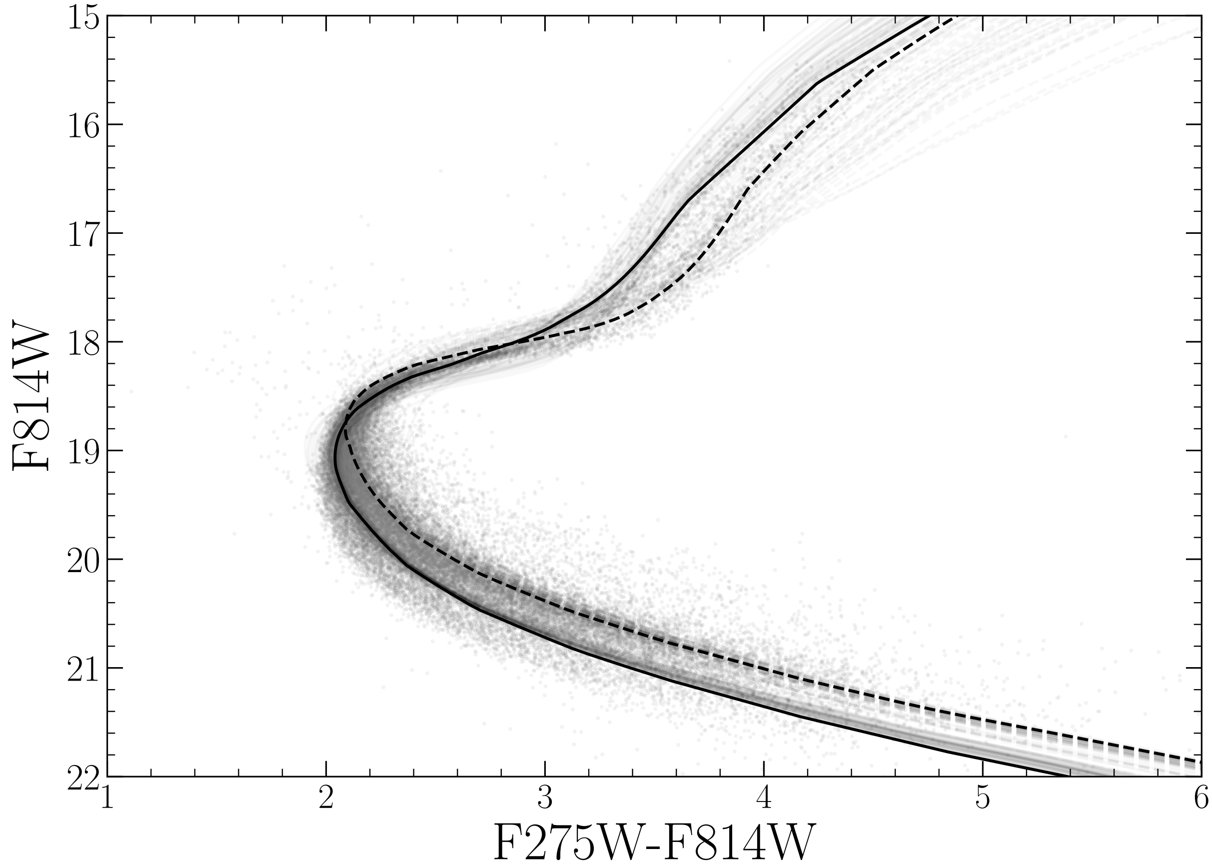

Figure 7. Best fit isochrone results for NGC 2808. The best fit P1 and P2 models are shown as black lines. The following 50 best fit models are presented as grey lines. The dashed black line is fit to P1, while the solid black line is fit to P2.

Population	Age [Gyr]	Distance Modulus	Extinction [mag]	Y	α_{ML}	χ^2_ν
P1	$12.996^{+0.87}_{-0.64}$	15.021	0.54	0.24	2.050	0.021
P2	$13.061^{+0.86}_{-0.69}$	15.007	0.537	0.39	1.600	0.033

Table 1. Best fit parameters derived from fitting isochrones to the fiducual lines derived from the NCG 2808 photometry. The one sigma uncertainty reported on population age were determined from the 16th and 84th percentiles of the distribution of best fit isochrones ages.

formation from additional filters (F336W and F438W) which we do not use in our CMD approach. We preform the same analysis on the F336W-F438W CMD using `Fidanka` as we do on the F275W-F814W CMD. While the clustering algorithm does find a more strongly distinguished potential third population using these filters (Figure 8 bottom), the two population hypothesis remains strongly preferred. Moreover, the process of transforming magnitude measurements into chromosome space results in dramatically increased uncertainties for each star. We find a mean fractional uncertainty for chromosome parameters — $\Delta_{F275W,F814W}$ and $\Delta_{CF275W,F336W,F438W}$ — of ≈ 1 (Figure 9) when starting with magnitude measurements having a mean best-case (i.e. where the uncertainty is assumed to only be due to Poisson statistics) fractional uncertainty of ≈ 0.0005. Fractional uncertainties for chromosome parameters were calculated via standard propagation of uncertainty. Because of how `Fidanka` operates, i.e. resampling a probability distribution for each star in order to identify clusters, we are unable to make statistically meaningful statements from the chromosome map

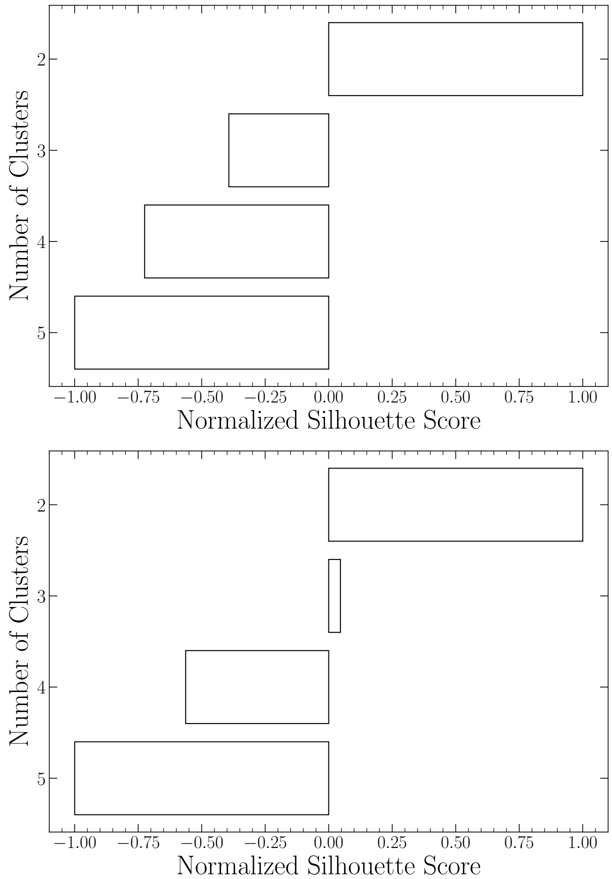

Figure 8. Silhouette analysis for NGC 2808 F275W-F814W (top) and F336W-F438W (bottom) photometry. The Silhouette scores are an average of score for each magnitude bin. Scores have been normalized to indicate the most well-distinguished (+1) to least well-distinguished (-1) hypothesizes.

6. CONCLUSION

Here we have performed the first chemically self-consistent modeling of the Milky Way Globular Cluster NGC 2808. We find that, updated atmospheric boundary conditions and opacity tables do not have a significant effect on the inferred helium abundances of multiple populations. Specifically, we find that P1 has a helium mass fraction of 0.24, while P2 has a helium mass fraction of 0.39. Additionally, we find that the ages of these two populations agree within uncertainties. We only find evidence for two distinct stellar populations, which is in agreement with recent work studying the number of populations in NGC 2808 spectroscopic data.

We introduce a new software suite for globular cluster science, `Fidanka` , which has been released under a permissive open source license. `Fidanka` aims to provide a statistically robust set of tools for estimating the parameters of multiple populations within globular clusters.

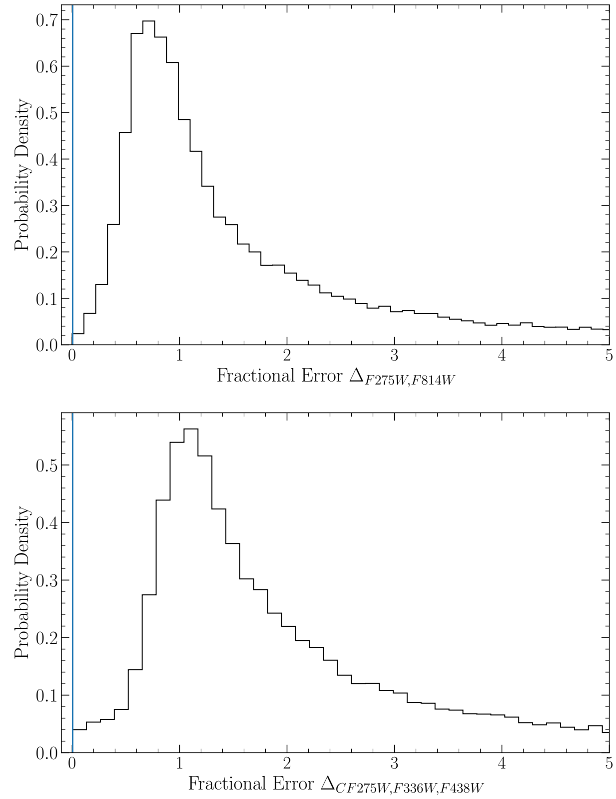

Figure 9. Fractional error distribution of $\Delta_{F275W,F814W}$ (top) and $\Delta_{CF275W,F336W,F438W}$. The vertical line near 0 in each figure indicates the mean fractional error of the magnitude measurements used to find the chromosome parameters.

This work has made use of the NASA astrophysical data system (ADS). We would like to thank Elisabeth Newton and Aaron Dotter for their support and for useful discussion related to the topic of this paper. We would like to thank the reviewers of this work for their careful reading and critique which has significantly improved this article. Additionally, we would like to thank Kara Fagerstrom, Aylin Garcia Soto, and Keighley Rockcliffe for their useful discussion related to in this work. We acknowledge the support of a NASA grant (No. 80NSSC18K0634).

REFERENCES

Alcaino, G. 1975, A&AS, 21, 15

Anderson, J., Sarajedini, A., Bedin, L. R., et al. 2008, AJ, 135, 2055, doi: 10.1088/0004-6256/135/6/2055

Barber, C. B., Dobkin, D. P., & Huhdanpaa, H. 1996, ACM Transactions on Mathematical Software (TOMS), 22, 469
Bastian, N., & Lardo, C. 2015, MNRAS, 453, 357, doi: 10.1093/mnras/stv1661
Bastian, N., & Lardo, C. 2018, Annual Review of Astronomy and Astrophysics, 56, 83
Bekki, K., & Chiba, M. 2002, The Astrophysical Journal, 566, 245, doi: 10.1086/337984
Boudreaux, E. M., & Chaboyer, B. C. 2023, ApJ, 944, 129, doi: 10.3847/1538-4357/acb685
Boylan-Kolchin, M. 2018, MNRAS, 1423, doi: 10.1093/mnras/sty1490
Brodie, J. P., & Strader, J. 2006, Annu. Rev. Astron. Astrophys., 44, 193
Brown, J. H., Burkert, A., & Truran, J. W. 1991, ApJ, 376, 115, doi: 10.1086/170260
—. 1995, ApJ, 440, 666, doi: 10.1086/175304
Cadelano, M., Dalessandro, E., Salaris, M., et al. 2022, ApJL, 924, L2, doi: 10.3847/2041-8213/ac424a
Carretta, E. 2006, AJ, 131, 1766, doi: 10.1086/499565
—. 2013, A&A, 557, A128, doi: 10.1051/0004-6361/201322103
—. 2015, ApJ, 810, 148, doi: 10.1088/0004-637X/810/2/148
Carretta, E., Bragaglia, A., & Cacciari, C. 2004, ApJL, 610, L25, doi: 10.1086/423034
Carretta, E., Bragaglia, A., Gratton, R. G., et al. 2010, Astronomy & Astrophysics, 516, A55
Colgan, J., Kilcrease, D. P., Magee, N. H., et al. 2016, in APS Meeting Abstracts, Vol. 2016, APS Division of Atomic, Molecular and Optical Physics Meeting Abstracts, D1.008
de Mink, S. E., Pols, O. R., Langer, N., & Izzard, R. G. 2009, A&A, 507, L1, doi: 10.1051/0004-6361/200913205
Decressin, T., Meynet, G., Charbonnel, C., Prantzos, N., & Ekström, S. 2007, A&A, 464, 1029, doi: 10.1051/0004-6361:20066013
Denissenkov, P. A., & Hartwick, F. D. A. 2014, MNRAS, 437, L21, doi: 10.1093/mnrasl/slt133
D'Ercole, A., D'Antona, F., Ventura, P., Vesperini, E., & McMillan, S. L. W. 2010, MNRAS, 407, 854, doi: 10.1111/j.1365-2966.2010.16996.x
D'Ercole, A., Vesperini, E., D'Antona, F., McMillan, S. L. W., & Recchi, S. 2008, MNRAS, 391, 825, doi: 10.1111/j.1365-2966.2008.13915.x
Dotter, A. 2016, ApJS, 222, 8, doi: 10.3847/0067-0049/222/1/8
Dotter, A., Chaboyer, B., Jevremović, D., et al. 2008, The Astrophysical Journal Supplement Series, 178, 89
Dotter, A., Ferguson, J. W., Conroy, C., et al. 2015, MNRAS, 446, 1641, doi: 10.1093/mnras/stu2170
Ferguson, T. S. 1973, The annals of statistics, 209
Gratton, R., Sneden, C., & Carretta, E. 2004, ARA&A, 42, 385, doi: 10.1146/annurev.astro.42.053102.133945
Gratton, R. G., Carretta, E., & Bragaglia, A. 2012, Astronomy and Astrophysics Reviews, 20, 50, doi: 10.1007/s00159-012-0050-3
Gratton, R. G., Lucatello, S., Carretta, E., et al. 2011, A&A, 534, A123, doi: 10.1051/0004-6361/201117690
Grevesse, N., Asplund, M., & Sauval, A. J. 2007, SSRv, 130, 105, doi: 10.1007/s11214-007-9173-7
Gustafsson, B., Edvardsson, B., Eriksson, K., et al. 2008, A&A, 486, 951, doi: 10.1051/0004-6361:200809724
Hong, S., Lim, D., Chung, C., et al. 2021, AJ, 162, 130, doi: 10.3847/1538-3881/ac0ce6
Hudson, M. J., & Robison, B. 2018, Monthly Notices of the Royal Astronomical Society, 477, 3869, doi: 10.1093/mnras/sty844
Husser, T. O., Wende-von Berg, S., Dreizler, S., et al. 2013, A&A, 553, A6, doi: 10.1051/0004-6361/201219058
Jordán, A., Côté, P., West, M. J., & Marzke, R. O. 2002, ApJL, 576, L113, doi: 10.1086/343759
Kalirai, J. S., & Richer, H. B. 2010, Philosophical Transactions of the Royal Society of London Series A, 368, 755, doi: 10.1098/rsta.2009.0257
Kostogryz, N., Shapiro, A. I., Witzke, V., et al. 2023, Research Notes of the AAS, 7, 39, doi: 10.3847/2515-5172/acc180
Kravtsov, A. V., & Gnedin, O. Y. 2005, The Astrophysical Journal, 623, 650
Kurucz, R.-L. 1993, Kurucz CD-Rom, 13
Lardo, C., Salaris, M., Cassisi, S., & Bastian, N. 2022, A&A, 662, A117, doi: 10.1051/0004-6361/202243843
Latour, M., Husser, T. O., Giesers, B., et al. 2019, A&A, 631, A14, doi: 10.1051/0004-6361/201936242
Legnardi, M. V., Milone, A. P., Armillotta, L., et al. 2022, MNRAS, 513, 735, doi: 10.1093/mnras/stac734
Marigo, P., & Aringer, B. 2009, A&A, 508, 1539, doi: 10.1051/0004-6361/200912598
Marigo, P., Aringer, B., Girardi, L., & Bressan, A. 2022, ApJ, 940, 129, doi: 10.3847/1538-4357/ac9b40
Marino, A. F., Milone, A. P., Karakas, A. I., et al. 2015, Monthly Notices of the Royal Astronomical Society, 450, 815, doi: 10.1093/mnras/stv420
Martocchia, S., Dalessandro, E., Lardo, C., et al. 2019, Monthly Notices of the Royal Astronomical Society, 487, 5324, doi: 10.1093/mnras/stz1596
Milone, A. P., Piotto, G., Bedin, L. R., et al. 2012, ApJ, 744, 58, doi: 10.1088/0004-637X/744/1/58
Milone, A. P., Marino, A. F., Piotto, G., et al. 2015a, ApJ, 808, 51, doi: 10.1088/0004-637X/808/1/51

—. 2015b, MNRAS, 447, 927, doi: 10.1093/mnras/stu2446

Milone, A. P., Piotto, G., Renzini, A., et al. 2017, MNRAS, 464, 3636, doi: 10.1093/mnras/stw2531

Milone, A. P., Marino, A. F., Renzini, A., et al. 2018, MNRAS, 481, 5098, doi: 10.1093/mnras/sty2573

Pasquato, M., & Milone, A. 2019, arXiv e-prints, arXiv:1906.04983, doi: 10.48550/arXiv.1906.04983

Pedregosa, F., Varoquaux, G., Gramfort, A., et al. 2011, Journal of Machine Learning Research, 12, 2825

Peebles, P. J. E., & Dicke, R. H. 1968, ApJ, 154, 891, doi: 10.1086/149811

Peng, E. W., Ferguson, H. C., Goudfrooij, P., et al. 2011, The Astrophysical Journal, 730, 23

Piotto, G. 2018, HST UV Globular Cluster Survey ("HUGS"), STScI/MAST, doi: 10.17909/T9810F

Piotto, G., Bedin, L. R., Anderson, J., et al. 2007, The Astrophysical Journal Letters, 661, L53, doi: 10.1086/518503

Piotto, G., Milone, A. P., Bedin, L. R., et al. 2015, AJ, 149, 91, doi: 10.1088/0004-6256/149/3/91

Plez, B. 2008, Physica Scripta Volume T, 133, 014003, doi: 10.1088/0031-8949/2008/T133/014003

Prantzos, N., Charbonnel, C., & Iliadis, C. 2007, A&A, 470, 179, doi: 10.1051/0004-6361:20077205

Renzini, A. 2008, Monthly Notices of the Royal Astronomical Society, 391, 354, doi: 10.1111/j.1365-2966.2008.13892.x

Richer, H. B., Fahlman, G. G., Buonanno, R., et al. 1991, ApJ, 381, 147, doi: 10.1086/170637

Rousseeuw, P. J. 1987, Journal of Computational and Applied Mathematics, 20, 53, doi: https://doi.org/10.1016/0377-0427(87)90125-7

Salaris, M., & Cassisi, S. 2005, Evolution of stars and stellar populations (John Wiley & Sons)

Sandage, A. R. 1953, AJ, 58, 61, doi: 10.1086/106822

Shahapure, K. R., & Nicholas, C. 2020, in 2020 IEEE 7th International Conference on Data Science and Advanced Analytics (DSAA), 747–748, doi: 10.1109/DSAA49011.2020.00096

Smith, G. H. 1987, Publications of the Astronomical Society of the Pacific, 99, 67, doi: 10.1086/131958

Sneden, C., Kraft, R. P., Prosser, C. F., & Langer, G. 1992, The Astronomical Journal, 104, 2121

Suntzeff, N. B., & Kraft, R. P. 1996, AJ, 111, 1913, doi: 10.1086/117930

Valle, G., Dell'Omodarme, M., & Tognelli, E. 2022, A&A, 658, A141, doi: 10.1051/0004-6361/202142454

van den Bergh, S. 2010, The Astronomical Journal, 140, 1043, doi: 10.1088/0004-6256/140/4/1043

Ventura, P., & D'Antona, F. 2009, A&A, 499, 835, doi: 10.1051/0004-6361/200811139

Ventura, P., D'Antona, F., Mazzitelli, I., & Gratton, R. 2001, ApJL, 550, L65, doi: 10.1086/319496